

Soft Matter

Accepted Manuscript



This is an *Accepted Manuscript*, which has been through the Royal Society of Chemistry peer review process and has been accepted for publication.

Accepted Manuscripts are published online shortly after acceptance, before technical editing, formatting and proof reading. Using this free service, authors can make their results available to the community, in citable form, before we publish the edited article. We will replace this *Accepted Manuscript* with the edited and formatted *Advance Article* as soon as it is available.

You can find more information about *Accepted Manuscripts* in the [Information for Authors](#).

Please note that technical editing may introduce minor changes to the text and/or graphics, which may alter content. The journal's standard [Terms & Conditions](#) and the [Ethical guidelines](#) still apply. In no event shall the Royal Society of Chemistry be held responsible for any errors or omissions in this *Accepted Manuscript* or any consequences arising from the use of any information it contains.

Syneresis and delayed detachment in agar plates[†]

Thibaut Divoux,^{*a} Bosi Mao,^a and Patrick Snares^{*a}

Received Xth XXXXXXXXXXXX 20XX, Accepted Xth XXXXXXXXXXXX 20XX

First published on the web Xth XXXXXXXXXXXX 200X

DOI: 10.1039/b000000x

Biogels made of crosslinked polymers such as proteins or polysaccharides behave as porous soft solids and store large amount of solvent. These gels undergo spontaneous aging, called *syneresis* that consists in the shrinkage of the gel matrix and the progressive expulsion of the solvent. As a result, a biogel originally casted in a container often lose contact with the container sidewalls, and the detachment time is a priori difficult to anticipate since it may occur over variable time spans (from hours to days). Here we report on the syneresis phenomena in agar plates that consist in Petri dishes filled with a gel mainly composed of agar. Direct observations and speckle pattern correlation analysis allow us to rationalize the delayed detachment of the gel from the sidewall of the Petri dish. The detachment time t^* is surprisingly not controlled by the mass loss as one would intuitively expect. Instead, t^* is strongly correlated to the gel minimum thickness e_{min} measured along the sidewall of the plate, and increases as a robust function of e_{min} independently of the prior mass-loss history. Time-resolved correlation spectroscopy atypically applied to such weakly diffusive media gives access to the local thinning rate of the gel. This technique also allows us to detect the gel micro-displacements that are triggered by the water evaporation prior to the detachment, and even to anticipate the latter from a few hours. Our work provides observables to predict the detachment time of agar gels in dishes, and highlights the relevance of speckle pattern correlation analysis for the quantitative investigation of the syneresis dynamics in biopolymer gels.

1 Introduction

Biogels formed through the self-assembling of polymers such as polysaccharides or proteins are widespread in manufactured goods and biomimetic products^{1,2}. Fields of applications range from food engineering where biopolymers are used as gelling agents³, to biotechnology where these gels commonly serve as growth media for microorganisms or as porous scaffold in tissue engineering^{4,5}. Biogels exhibit a porous microstructure made of an interconnected network that is a priori efficient to retain solvents. However, these structures are often metastable. Indeed, the constituents experience attractive interactions and biogels spontaneously rearrange and shrink on durations ranging from hours to days depending on the ambient relative humidity, leading to the progressive release of the solvent initially trapped. This phenomenon coined *syneresis* has been reported in biogels such as gelatin⁶, polysaccharide gels⁷, globular protein gels^{8–10}, organogels¹¹ and hydrogels from pNIPAM microgels¹², and more generally in colloidal gels that display weak attractive interactions^{13,14}. If the latter category of gels has been the topic of numerous studies, only a handful of paper have reported quantitative measure-

ments on the shrinkage dynamics of biogels, while the parameters controlling the detachment of a biogel from the preparation container stands as an open issue despite its outstanding practical importance.

Here we report on the syneresis process in commercial agar plates used as growth media for microorganisms or cells in routine diagnostic tests. These plates are usually incubated at constant temperature of about 35 to 40°C for several hours. Excessive syneresis leads to the gel detachment from the sidewall of the Petri dish which makes it hard to assess any bacterial growth and invalidates the test. This simple detachment issue delays each year the analysis of thousands of diagnostics and costs a fair share of money to medical companies due to customer return. The gelling constituent of these plates is agarose, a hydrophilic colloid extracted from seaweeds⁷, which formation and structural properties have been thoroughly investigated over the past 40 years^{15–17}. Insoluble in cold water, agar becomes soluble in boiling water and, once cooled down below 40°C, forms a thermoreversible gel that does not melt below 80°C. For concentrations above 1% (w/w) as it is the case for agar plates, the gel is formed through a competition between a spinodal demixing process and the association of molecules in double helices^{18–21}. This process leads to a fibrous fractal-like microstructure that is controlled by the agarose concentration²² and the thermal history^{23,24}. Such scale free microstructure reflects in their linear mechanical properties as the gel elastic modulus increases as weak

[†] Electronic Supplementary Information (ESI) available: [A movie and three supplemental figures together with their descriptions and explanations]. See DOI: 10.1039/b000000x/

^a Université Bordeaux, Centre de Recherche Paul Pascal, UPR 8641, 115 av. Dr. Schweitzer, 33600 Pessac, France

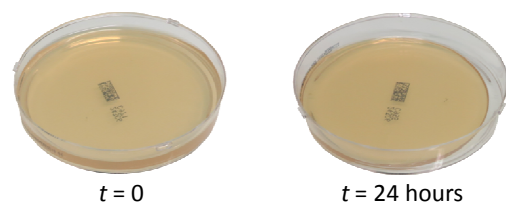


Fig. 1 Commercial agar plate from a fresh batch (left) and after a 24h incubation at 25°C (right). The gel has detached from the sidewall on the right side of the dish. The scale is set by the dish diameter of 8.5 cm.

power-law of the frequency^{25,26}. Agar gels behave as soft solids and display a brittle-like rupture scenario under large strains that involves macroscopic fractures, while considerable creep occurs under external stress before a delayed rupture²⁷. Agar gels are also subject to ageing together with the spontaneous release of water. Such syneresis phenomenon is attributed to the contraction of the polymer network by a slow further aggregation of the helices^{28,29} and is enhanced under external stress⁷, or low humidity conditions. Quantitative measurements of syneresis in agar gels merely consist in weighing the solvent-loss³⁰ and most of the current knowledge is limited to empirical laws regarding the influence of the gel composition: syneresis in agar gels goes roughly as the inverse square root of the polymer concentration⁷, while tuning the internal hydrophobicity of the gel by incorporating water-binding components such as sucrose³¹, ester sulfate¹⁷, xanthan³², or locust bean gum³³ may delay and/or prevent part of the water release.

In this article, we focus on the delayed detachment of agar gels in plastic Petri dishes that is triggered by the syneresis. The detachment is named *delayed* as it may occur from a few hours up to 30 hours, from the moment the plates are opened and incubated at constant temperature. Direct visualization and speckle pattern correlation experiments allow us to analyze the gel dynamics before its detachment from the sidewall of the dish, and to identify the key parameters controlling the detachment time t^* . Surprisingly, t^* is not controlled by the water loss, as two gels of identical mass with different mass loss history may detach over very different timescales. Instead, the detachment time is strongly correlated to the gel thickness asymmetry along the plate periphery, and increases as a robust power law of the gel minimum thickness e_{min} independently of the gel prior history. Such simple quantities constitute promising macroscopic observables to estimate and optimize the shelf life of commercial plates. Time-resolved correlation experiments further allow us to measure the gel local thinning rate and demonstrate that despite the gel detachment occurs in a sudden single step, it can be anticipated from a few hours by monitoring the gel micro-displacements while

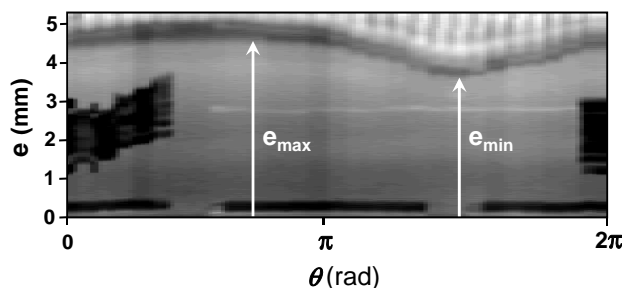


Fig. 2 Panoramic sideview of a commercial agar plate ($m = 26$ g). The image is built by rotating the plate in front of a webcam and stacking consecutive vertical snapshots recorded at regular angle intervals. The representation $e(\theta)$ illustrates the variations of the gel thickness e along the periphery of the Petri dish ($e_{min} = 3.58 \pm 0.03$ mm and $\delta e = e_{max} - e_{min} = 1.02 \pm 0.03$ mm). The image height is about 800 pixels and the black inscription is the plate serial number.

it is still in contact with the sidewall of the dish.

2 Materials and methods

2.1 Agar plate samples

The samples consist in gamma-irradiated sterile agar plates (Fig. 1) commercialized by BioMérieux as microbiological growth media[‡]. Plates are made of a cylindrical plexiglas box (diameter 8.5 cm, height 1 cm) covered with a removable lid and are partially filled with an agar gel (1.5 % w.t.) containing nutrients for bacterial growth that include peptones, sodium salts, etc.

As a first key observation, one can notice that the gel thickness is not homogeneous, especially along the sidewall of the Petri dish. This point is of primary importance for the dynamics of the gel detachment from the dish as will be discussed in section 3.1. Prior to any use, each plate is weighted to determine the mass m of gel it contains, and the gel thickness $e(\theta)$ along the sidewall of the Petri dish is measured by means of a webcam (Logitech HD c920) with an accuracy of ± 30 μm . In particular, we record the gel minimum and maximum thicknesses, resp. e_{min} and e_{max} (Fig. 2). For the samples investigated here, the gel mass m ranges from 21 to 27 g, while the gel thickness asymmetry $\delta e \equiv e_{max} - e_{min}$ lies between 0.3 and 1.4 mm for a typical average thickness of about 4 mm. Both the gel weight m and thickness $e(\theta)$ depend upon the gel casting process on the production line, and therefore are not con-

[‡] Note that gamma irradiation is performed after gelation to sterilize the plates. To our knowledge, there are no studies dealing with the effect of post-gelation irradiation on the mechanical properties of agar gels. Nonetheless, note that irradiation of agar prior to gelation is known to impact the gel mechanical properties by lowering the gel failure stress compared to non-irradiated samples³⁴.

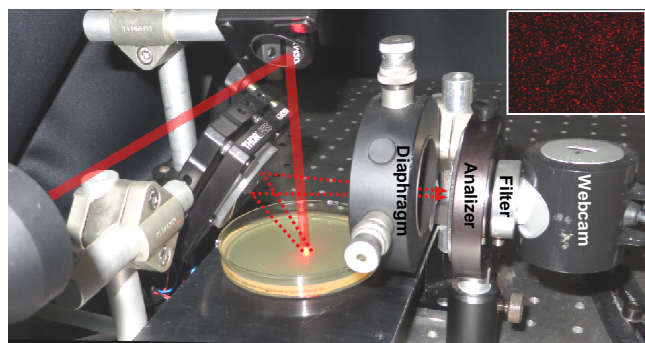


Fig. 3 Photography of the optical setup used to record the speckle pattern from the agar plate in the backscattering geometry. The laser beam trajectory has been sketched in red for the sake of clarity. Inset: typical speckle pattern.

control parameters in this study. This is why we have performed experiments on a large number of plates to sample different values of m and e . As a result of water exudation and evaporation, m and e progressively decrease up to the point the gel detaches from the lateral wall of the dish and further retracts [Fig. 1 (right)] which marks the end of the product shelf life. Commercial agar plates come in batches of 10 plates wrapped together. To test the reproducibility of our results, each experiment is repeated on several independent batches which exact number is given in the text.

2.2 Direct visualization

For each batch, the 10 plates are placed at the same level on top of a grid inside a programmable testing chamber (Binder MK53) that maintains a constant temperature of $(25.0 \pm 0.1)^\circ\text{C}$ and a relative humidity of about 50%. Plates are monitored over several hours (up to ~ 40 hours) with a webcam (Logitech HD c920) placed inside the chamber and used in timelapse mode with a frame rate of 1 image per minute.

2.3 Time correlation spectroscopy

The gel dynamics of a single plate can also be monitored through speckle pattern correlation in a room thermostated at $(25.0 \pm 0.1)^\circ\text{C}$ and with a humidity level of about 50%. The optical setup pictured in figure 3, consists in a linearly polarized laser beam (He-Ne Melles Griot gas laser, 20 mW at $\lambda = 632.8$ nm) that is expanded to 5 mm with a collimator and directed perpendicularly to the sample by means of a mirror. The light is backscattered from the center region of the plate (illuminated volume ~ 100 mm³) and forms a speckle pattern on a low sensitivity CCD array (Webcam Phillips SPC900NC, 640 \times 480 pixels) an example of which is represented in the inset of figure 3. To remove the ambient light, an interference

filter is placed in front of the detector and for each experiment, the angular position of the plate and the diaphragm aperture are tuned to spread the intensity range over the whole accessible grayscale of the detector, and obtain an autocorrelation radius (\sim speckle grain radius) of about 3 pixels. We have checked that the results reported here do not depend on the exact position of the enlightened volume in the sample.

As water evaporates, the gel thins and the speckle pattern changes. The degree of correlation between two speckle images separated by a lag time τ is determined by the ensemble-average intensity correlation function $g_2(t, \tau)$ defined as follows:

$$g_2(t, \tau) = \frac{\langle I_p(t) \cdot I_p(t + \tau) \rangle_p}{\langle I_p(t) \rangle_p \cdot \langle I_p(t + \tau) \rangle_p} \quad (1)$$

where I_p denotes the brightness level of pixel p and $\langle \dots \rangle_p$ an ensemble average over all the pixels³⁵. The correlation function is further normalized into a function noted $g_2^*(t, \tau)$ that verifies the condition $g_2^*(t, \tau = 0) = 1$. Here, $g_2^*(t, \tau)$ is computed at a frame rate of 10 Hz over a lag time τ ranging from 0 to 1 min. Speckle patterns are processed in real time by means of a custom-made java plug-in with the NIH Image processing package, and speckle images are only saved every minute for a lag time $\tau = 0$ to avoid storing too large amount of data³⁶.

The gel is a weakly scattering media and the speckle pattern is mainly produced by the interference of the light beam initially polarized, that is either reflected by the air/gel interface and/or by the gel/dish bottom interface. The polarization of the light reflected by the air/gel interface is unchanged, whereas the polarization of the light reflected by the gel/dish bottom interface is modified, as the Petri dish is made out of a birefringent material. To take advantage of this situation, an analyzer is placed in front of the webcam (Fig. 3) and is oriented either parallel or perpendicular to the original polarisation direction. To illustrate the speckle evolution in each of these two configurations, we report an experiment on an agar plate which first (second resp.) half is performed in the parallel (perpendicular resp.) configuration [Fig. 4(a)].

In the parallel configuration, the speckle results from the interference of the light reflected at the air/gel interface and at the gel/bottom plate interface and its decorrelation is mainly due to the gel thinning. Quantitatively, the correlation function $g_2^{*//}$ reported in figure 4(b) decreases rapidly over a timescale $\tau_d^{*//} \simeq 5$ s and further displays a periodic modulation $\tau_M^{*//}$ of about 8 s that is also clearly visible in the dynamics of the lag-time temporal diagram of the correlation function [Fig. 4(a), for $t < 6.3$ h]. On the one hand, the short time decorrelation is induced by any change of $\lambda/2$ in the two optical paths. Indeed, a constant evaporation rate $\dot{m} = 0.7$ g/hour at 25°C (see table 1 in section 3.1) of a cylindrical gel of radius $R = 4.2$ cm and density $\rho = 1000$ kg/m³ leads to $\tau_d^{*//} = \lambda \rho \pi R^2 / (4 \dot{m}) \simeq 4.5$ s in agreement with the initial decay of $g_2^{*//}$ in figure 4(b). On

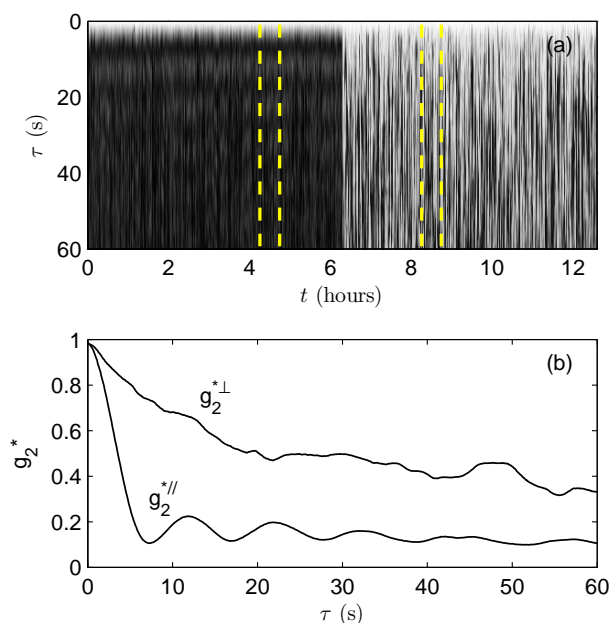


Fig. 4 (Color online) (a) Lag-time temporal diagram of the intensity correlation function $g_2^*(t, \tau)$ coded in grayscale as a function of the lag time τ , and the experimental time t . The first half of the experiment is performed with parallel polarizers ($t < 6.3$ hours) and the second half of the experiment with crossed polarizers ($t \geq 6.3$ hours). The detachment of the gel from the sidewall of the dish occurs later at $t = 16$ hours (data not shown). (b) Intensity correlation function g_2^* vs. the lag time τ extracted from (a) at $t = 4.5$ hours (parallel configuration) and at $t = 8.5$ hours (crossed configuration) and averaged over a time window of $\Delta t = 30$ min [duration enclosed between the yellow dotted lines in (a)]. The gel characteristics are the following: $m = 26$ g, $e_{min} = 3.74$ mm and $\delta e = 0.75$ mm.

the other hand, the modulation of the correlation function is caused by the constructive interference due to the gel thinning. Two successive maximum of the intensity correlation function $g_2^{*//}$ correspond to a change Δ in the optical paths of photons either reflected at the air/gel interface or at the dish bottom such as $\Delta = 2nd = \lambda$, where d denotes the decrease in the gel thickness, and n stands for the refractive index of the gel very close to that of water ($n \approx 1.33$). As the air/gel interface goes down at a velocity $v = \dot{m}/(\rho\pi R^2) = d/\tau_M^//$, we can estimate the period of the oscillations to be $\tau_M^// = \lambda/(2nv) \approx 7$ s, in agreement with the modulation period of $g_2^{*//}$ [Fig. 4(b)].

In the perpendicular configuration, the webcam barely receives the light reflected at the air/gel interface which polarization is orthogonal to its initial value, and is now filtered by the analyzer. Therefore, in this configuration the speckle pattern is far less sensitive to the displacement of the air/gel interface and it decorrelates much more slowly than in the parallel con-

figuration [Fig. 4(b)]. Nonetheless, the decorrelation still occurs and results from (i) the micro-displacement of the gel inside the dish[§] while the gel thins but remains macroscopically in contact with the sidewall, and from (ii) the local changes in the surface topography or in the orientation of the air/gel interface induced by the aforementioned displacements.

The micro-displacements of the gel within the dish are triggered by the successive relaxations of the internal stress. The latter progressively builds up as the gel tends to contract due to water evaporation, but sticks to the sidewall. The average internal stress increases up to the moment the contraction forces overcome the adhesion forces between the gel and the sidewall leading to the sudden detachment. Therefore, in the perpendicular configuration, the temporal evolution of the speckle reflects the gel dynamics well before the detachment and allows us to infer the micro-displacement of the gel during the syneresis. Furthermore, in this configuration one can see in figure 4(a) (for $t \geq 6.3$ h) that the speckle decorrelates over a timescale that varies considerably, from seconds to minutes, which suggests that the occurrence of these micro-displacements is intermittent. A more detailed analysis of these fluctuations reported in section 3.2 confirms this interpretation and reveals that TRC allows us to detect precursors to the gel detachment from sidewall of the dish.

3 Results

3.1 Macroscopic approach

In a first series of experiments, a batch of 10 plates without their lids is placed in a thermoregulated chamber ($T = 25^\circ\text{C}$) and left at rest. Water evaporates from the agar plate and the gel stay still for several hours before suddenly detaching from the sidewall of the Petri dish at a time noted t^* [See movie 1 in the supplemental material]. After detaching, the gel shrinks and although the gel may lose up to 40 % of its initial weight during the syneresis, we observe no sign of failure or fracture at any time[¶].

To identify the control parameters of the gel detachment during the early stage of the syneresis, we report in figure 5 the evolution of the gel detachment time versus the gel initial characteristics. As a key result, t^* is observed to increase as a power law of the gel minimum thickness e_{min} , measured

[§] Note that the displacement responsible for the speckle decorrelation is due to the micro-displacement of the gel and also to the deformation of the Petri dish under the forces exerted by the gel that contracts, because of the water evaporation. We have checked that the use of a rigid container (e.g. a Petri dish made of glass instead of plastic) somewhat dampens the temporal fluctuations of the speckle pattern observed in perpendicular configuration [see Fig. 1 in the supplemental material].

[¶] Note that, pushing the experiments forward, the gel turns into a thin and dry buckled pancake that can be rejuvenated by adding water. The gel then swells and recovers its initial cylindrical shape, occupying the whole Petri dish after a few hours (data not shown).

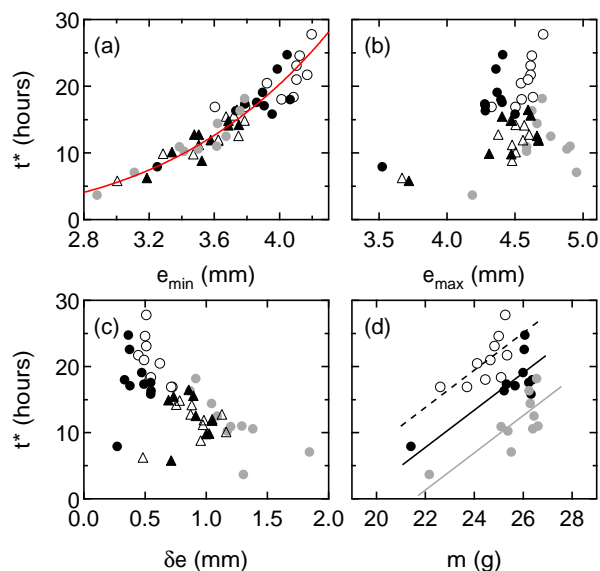


Fig. 5 (Color online) Detachment time t^* of the gel from the sidewall of the Petri dish plotted vs the value measured at $t = 0$ of (a) the gel minimum thickness e_{min} , (b) the gel maximum thickness e_{max} , (c) the thickness asymmetry $\delta e = e_{max} - e_{min}$ and (d) the gel weight m . The red curve in (a) is the best power-law fit of the data that passes through the origin: $t^* = 4 \cdot 10^{-2} e_{min}^{4.5}$. The lines in (d) are guides for the eye. Symbols (\circ), (\bullet) and (\blacklozenge) stand for two independent batches of 10 plates each used in direct visualization experiments, while (Δ) and (\blacktriangle) stand for three independent batches of 10 plates for which t^* was determined by correlation spectroscopy experiments (see section 3.2).

along the sidewall of the Petri dish [Fig. 5(a), (\circ), (\bullet) and (\blacklozenge)]. This relation is robustly verified over 30 plates of different initial weights and mass loss history. By contrast, the detachment time is not correlated to the gel maximum thickness [Fig. 5(b)]. Moreover, the detachment time also increases with the mass of the gel [Fig. 5(d)]. Nonetheless, if the data obtained with the same batch can be described with a single increasing function of m , two gels with the same initial mass but taken from different batches may detach over very different timescales. This last observation is likely related to the fact that plates from different batches may have been exposed to different storage conditions and may have lost various amount of water since their production. Last but not least, the detachment time also appears to be correlated to the amplitude of the variations of the gel thickness quantified by $\delta e = e_{max} - e_{min}$, but to a lesser extent as the data are more scattered than for t^* vs e_{min} [Fig. 5(c)]. One should nonetheless keep in mind that gels with larger thickness asymmetry are more likely to detach sooner from the sidewall.

Beyond the detachment time, we have monitored the evolution of the gel thickness and the weight of the Petri dishes

Temperature ($^{\circ}\text{C}$)	$\delta\dot{m}$ (g/hour)
20	0.50 ± 0.02
30	0.86 ± 0.03
40	1.81 ± 0.08

Table 1 Mass loss rate $\delta\dot{m}$ determined at three different temperatures T . Each value is the result of a linear fit of $\delta m(t) = m(0) - m(t)$ for 6 different plates extracted from three different batches. Measurements are detailed in figure 2 in the supplemental material.

stored in the thermoregulated chamber. The experiments show that the water loss increases linearly with time, while the gel detachment does not affect the mass-loss rate (see Fig. 2 in the supplemental material). This result is robust and experiments performed at larger temperatures simply lead to similar results with larger loss-rates (Table 1). Moreover, the average thickness of the gel decreases linearly in time in agreement with the evolution of the mass loss, while the thickness asymmetry δe remains about constant up to the detachment (see Fig. 3 in the supplemental material). The latter result urges to have a closer look at the gel dynamics where the gel thickness is minimal.

The temporal evolution of the gel thickness, at the very location where the detachment takes place is reported in figure 6 (a)–(f). One can see that the gel also thins linearly with time at this specific location. However, about one hour before the detachment, the thinning speeds up in this spot as evidenced in the spatio-temporal diagram displayed in figure 6(f) and the growth of a lens-shaped meniscus [Fig. 6(e)] finally leads to the detachment of the gel from the sidewall. This observation appears as robust and confirms that this specific area of the gel in contact with the sidewall of the dish plays a key role in the detachment process and necessitate more sensitive measurements.

3.2 TRC study of the syneresis

To get deeper insights on the gel dynamics and in particular on the local displacements that the gel experiences before the detachment, we performed a series of speckle pattern correlation experiments. An agar plate is placed at $T=25^{\circ}\text{C}$ in the custom made optical setup described in section 2.3 which is set in the perpendicular configuration to filter the light reflected at the air/gel interface and avoid the short time decorrelation of the speckle. The gel dynamics during the water evaporation is quantified by computing the intensity correlation function $g_2^{*\perp}(t, \tau)$ over a lag time $\tau = 1$ min repeatedly, during 10 to 30 hours (including during and after the macroscopic detachment).

Figure 7(a) displays the lag-time temporal diagram of the correlation function $g_2^{*\perp}(t, \tau)$ coded in grayscale. One can see that $g_2^{*\perp}(t, \tau)$ exhibits two different regimes that point toward

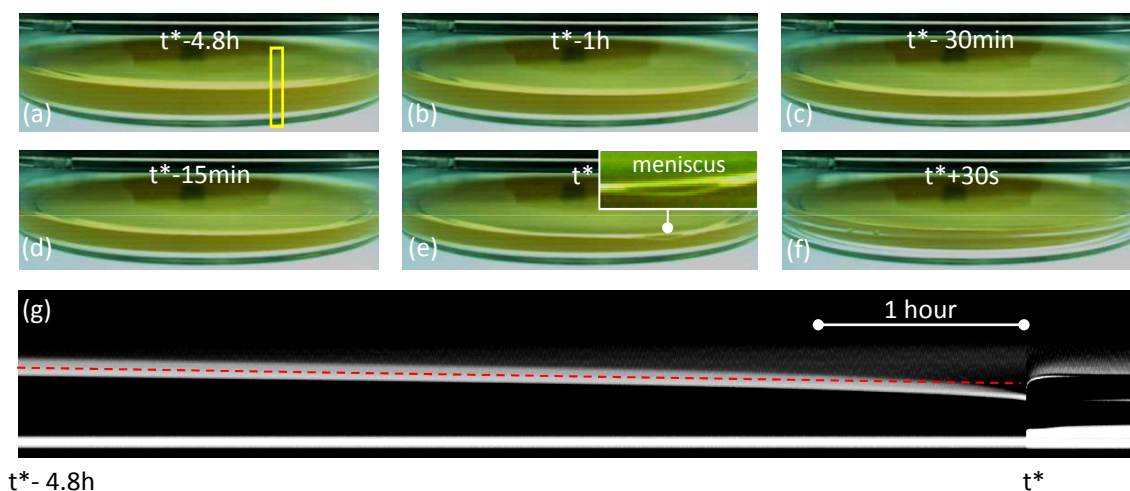


Fig. 6 (a)-(f) Sideview images of a gel in a Petri dish during the syneresis, taken at different times before and after the detachment of the gel from the sidewall of the dish. Note in (e) the appearance and the growth of a lens shaped meniscus at the exact location where the detachment will occur at $t^* = 4.8$ hours. (f) Spatiotemporal diagram of the gel thickness $e(t)$ as a function of time and computed in the region of interest emphasized by a yellow frame in (a) which corresponds to the detachment location. As shown by the red dashed line (guide for the eye), the gel thickness decreases linearly with time in this region, up to one hour before the detachment. Then, the gel thinning speeds up concomitantly with the growth of a lens shaped meniscus visible in (e) before the gel detachment. The gel characteristics are: $m = 23.8$ g, $e_{min} = 3.15$ mm and $\delta e = 1$ mm.

a dramatic event at a specific timescale $t = t^*$ [red dashed line in fig. 7]. To compare this timescale to the detachment time measured by direct visualization experiments, we have carefully repeated the experiment for twenty agar plates from two batches, and the time t^* determined through TRC measurements is systematically reported vs. e_{min} in figure 5 [Symbols (Δ) and (\blacktriangle)]. All the data points fall on the exact same power-law dependence as found in section 3.1, which demonstrates that the time t^* derived from the local measurements coincides with the macroscopic detachment time identified by direct visualization experiments.

Before and after t^* , the correlation function displays different behaviors that reflect two distinctive dynamics of the gel. For $t < t^*$, the gel sticks to the sidewall of the dish, and due to water evaporation, the air/gel interface is stretched and flat. In the perpendicular configuration, the light reflected at this interface is mostly filtered by the analyzer (section 2.3) and the correlation function reflects the micro-displacement of the gel that we discuss in more details in the following paragraph. For $t > t^*$, the gel has detached from the sidewall and is free to contract. The periodic modulation of the correlation function of about $\tau \approx 25$ s [Fig. 7(a) for $t > t^*$] is due to the gel thinning^{||}. This interpretation is further supported by a sup-

plemental experiment performed on a fresh plate which gel has been carefully detached from the sidewall of the dish by means of a cutter blade, before the start of the experiment (see Fig. 4 in the supplemental material). In that case, the correlation function displays, from $t = 0$, a modulation very similar to the one reported for a standard gel after it has detached (i.e. for $t > t^*$).

Let's turn now to the gel micro-displacements that take place before the detachment by having a closer look at $g_2^{*\perp}(t, \tau)$ for $t < t^*$ [Fig. 7(b)]. As mentioned in section 2.3, in the crossed polarizers configuration, the speckle decorrelation results from the micro-displacements of the gel within the dish that drive the speckle dynamics at short lag times ($\tau \leq 30$ s, see Fig. 5 in the supplemental material), and from the local subsequent changes in the topography or orientation of the air/gel interface that lead to the complete decorrelation of the speckle at longer times. Therefore, here we focus on the temporal evolution of $g_2^{*\perp}(t, \tau)$ for $\tau \leq 30$ s. We have computed for three different plates, the probability distribution function (PDF) of $g_2^{*\perp}(t, \tau)$ pictured in semi-logarithmic scale in figure 8(a) at $\tau = 0.5, 2$ and 10 s. The PDF remains nearly Gaussian for short lag times $\tau \leq 0.2$ s, while $g_2^{*\perp}(t, \tau)$ explores smaller values for increasing values of the lag time, and the distribution $P(g_2^{*\perp})$ develops an exponential tail [Fig. 8(a)]. The data located to the right of the maximum are fitted by a Gaussian function

period to be $\tau_M^\perp = \lambda/[2(n-1)v] \approx 30$ s, which is consistent with the experiments.

^{||} Indeed, two successive maximum of the intensity correlation function $g_2^{*\perp}$ correspond to a change of $\Delta = \lambda/[2(n-1)]$ in the optical paths of the photons reflected at the gel/dish bottom interface. Estimating the gel thinning speed v from the mass loss rate \dot{m} (see section 2.3), one may derive the modulation

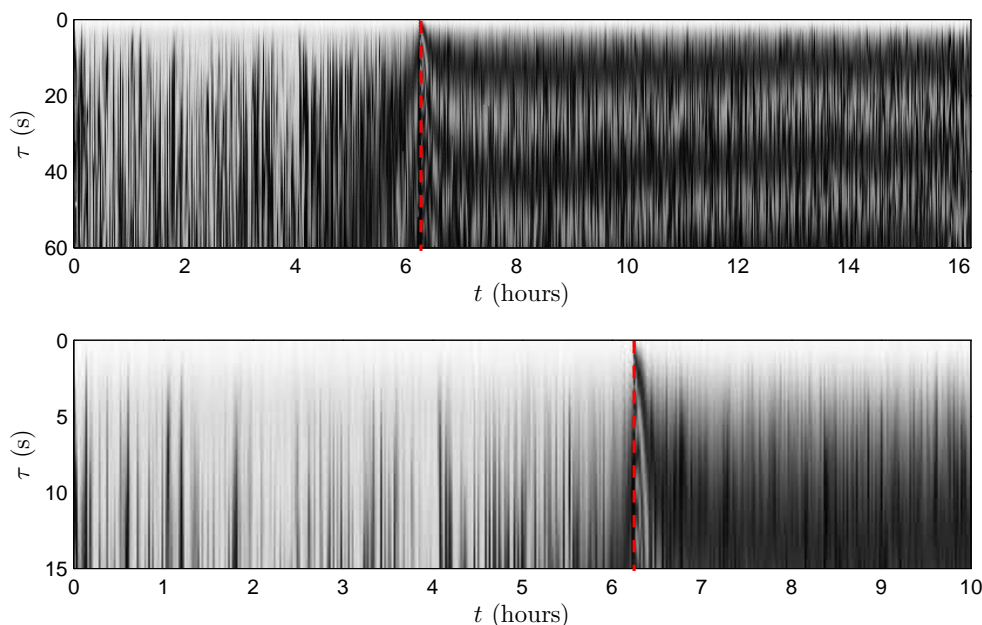


Fig. 7 (a) Lag-time temporal diagram of the intensity correlation function $g_2^{*\perp}(t, \tau)$ coded in grayscale and measured in the perpendicular configuration, as a function of the lag time τ and the experimental time t . The vertical red dashed line at $t \equiv t^* = 6.25$ hours indicates the time at which the gel detaches from the sidewall of the Petri dish. For $t \leq t^*$, the speckle decorrelates over a fluctuating timescale due to the micro-displacements of the gel in contact with the sidewall of the dish. For $t > t^*$, the gel is free to contract and the speckle decorrelates more rapidly. The modulation of $g_2^{*\perp}$ of about 20 s is related to the gel thinning (see text). (b) Zoom over the early stage of the lag-time temporal diagram, for short lag times. The gel characteristics are: $m = 21.64$ g, $e_{min} = 3.18$ mm and $\delta e = 0.48$ mm.

which center $\langle x \rangle$ and variance σ are reported in figures 8(b) and (c) for twenty plates. Both parameters are independent of the detachment time of the gel which demonstrates that the gel dynamics on short time scale is thermally controlled by water evaporation and not related to the sudden macroscopic detachment. The latter is more likely the result of the accumulation of micro-displacements. This result also suggests that the Gaussian part of the distribution is related to random micro-displacements that do not lead to the gel relaxation on short timescales. In this framework, the growth of a non-Gaussian tail to the distribution of $g_2^{*\perp}$ for $\tau \geq 2$ s is related to irreversible micro-displacements of the gel relative to the dish that relax adhesion forces between the gel and the sidewall. The amount of these micro-displacements for a given lag time τ can be assessed by computing the fraction of data points δ in the PDF $P(g_2^{*\perp})$ that lays outside the Gaussian fit. One can see in the inset of figure 8(a) that δ neither depends on the plate nor on the gel detachment time, and increases with the lag time to reach $\sim 60\%$ at $\tau = 10$ s. This timescale is comparable to the half modulation period $\tau_M^{\perp}/2 \approx 12$ s measured during gel thinning in the perpendicular configuration, and after the detachment from the dish has occurred [Fig. 4(a), $t > t^*$] which confirms

that these gel irreversible micro-displacements are driven by water evaporation.

Finally, the last but not least remarkable feature of the lag-time temporal diagram pictured in figure 7(a), is that the decorrelation rate of the speckle pattern strongly increases about two hours before the gel detachment. The decorrelation time defined as the lag time τ^* for which $g_2^{*\perp}(t, \tau^*) = g_2^{*\perp}(t, 0)/e$ is plotted in figure 9 as a function of the elapsed time $t - t^*$ for three plates that display very different detachment times t^* ranging from 6 to 14 hours. For $t^* - t \gtrsim 2.5$ h, τ^* exhibits large fluctuations around a constant mean value of about 0.7 min in agreement with the fact that the evaporation rate is constant and the gel thickness decreases linearly in time (section 3.1). For $t^* - t \lesssim 2.5$ h, τ^* decreases as a robust power-law that scales as $(t^* - t)^{0.75}$ independently of the detachment time (inset of Fig. 9). This result shows that the number and/or the amplitude of the gel micro-displacements within the dish increases in a robust fashion up to the detachment. Such increase in the gel activity is also probably related to the formation and the growth of the lens-shaped meniscus in the vicinity of the sidewall at the location where the detachment later takes place [Fig. 6(e) and (g)]. Furthermore,

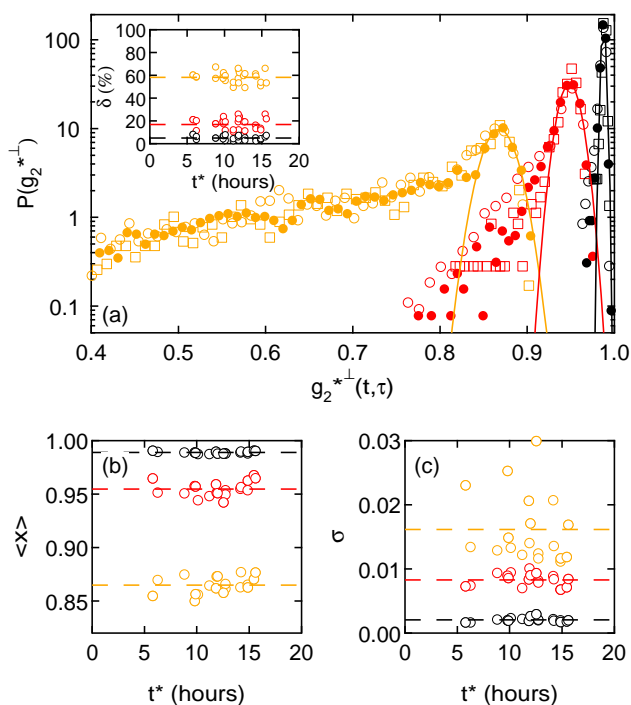


Fig. 8 (Color online) (a) Probability distribution function of $g_2^{*±}(t, \tau)$ computed at $\tau = 0.5, 2$ and 10 s from right to left, for three different plates (same symbols as in fig. 9). For (□) the distribution is computed for t ranging between 20 min and 3 hours, while for (○) and (●) the distribution is computed between 20 min and up to 8 hours. Inset: fraction δ of data values that lays outside the Gaussian fit of the data reported in (a) vs the detachment time. (b) Mean value $\langle x \rangle$ and (c) variance σ extracted from Gaussian fits for twenty different plates and plotted vs. the detachment time. Horizontal dashed lines stand for the mean values of the data.

such power-law scaling is reminiscent of the finite time singularity reported for the breakup of liquid droplets³⁷ and could be the signature of the fission at $t = t^*$ of the liquid film located between the gel and the sidewall. Indeed, we checked by means of a homemade compression cell that small deformations of about 3 to 5% are sufficient to trigger the release of water from the gel. Therefore, one can easily imagine that the stresses generated by evaporation between the gel and the sidewall may form such liquid film. This last point is left for future work.

4 Discussion and outlooks

Agar plates display syneresis and water evaporation which lead to the delayed detachment of the gel from the sidewall of the dish. Water loss appears as a continuous process that is not affected by the gel detachment, and which rate increases

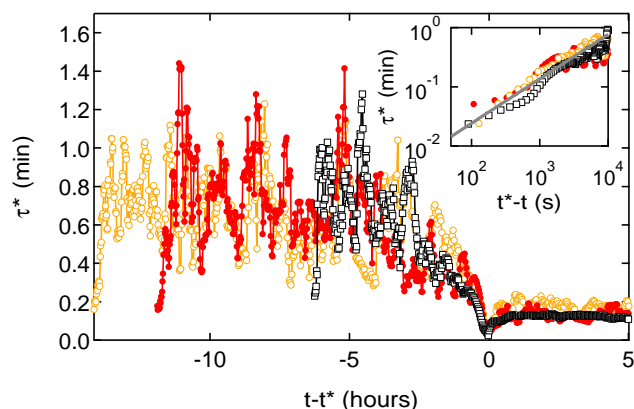


Fig. 9 (Color online) Evolution of the decorrelation time τ^* defined as $g_2^{*±}(t, \tau^*) = g_2^{*±}(t, 0)/e$ vs. $t - t^*$, the elapsed time centered on the detachment time t^* . Each point is an average over $\Delta t = 10$ min. Symbols stand for different plates: (□) is the same plate as reported in fig. 7 which gel detaches at $t^* = 6.248$ hours, while (○) and (●) display detachment times respectively of $t^* = 14.16$ hours and 11.89 hours. Inset: Same data replotted vs. $t^* - t$ in logarithmic scale in the vicinity of the detachment. The line is the best power-law fit of the data: $\tau^* \propto (t^* - t)^{0.75}$.

for increasing temperatures. The gel thickness decreases linearly up to the detachment which occurs at the exact angular location where the gel thickness was originally minimal. As a key result confirmed by both local and global measurements, the detachment time itself is strongly correlated to the gel minimum thickness, independently of the prior mass-loss history of the gel. It suggests that the detachment is governed rather by the adhesion of the gel to the dish, than by the water loss. Speckle pattern correlation experiments give access to the local thinning rate of the gel that is about a few 10 nm/s, and show that the gel experiences micro-displacements induced by the water loss. As water evaporates, the gel tends to contract but remains in contact with the sidewall of the dish due to weak adhesion forces. The stress builds up which triggers irreversible micro-displacements up to the sudden detachment at $t = t^*$. The amplitude and/or the number of these displacements increases dramatically a few hours before t^* which diminishes the decorrelation time of the speckle and makes it possible to anticipate the detachment by TRC analysis.

However, the exact location and the spatial extent of the gel micro-displacements inside the dish remains an open question: they could be located at the bottom of the dish or at the sidewall. Furthermore, if there is no doubt that the weak adhesion forces between the gel and the sidewall of the dish strongly impact the detachment time, the exact role of the friction properties between the gel and the dish bottom stands as an open issue. Future experiments will involve simultaneous TRC ex-

periments in various region of interest and Photon Correlation Imaging³⁸ to map the gel displacements over the dish bottom prior to the detachment.

Finally, a local scenario of the syneresis at the scale of a single pore of the gel and in presence of evaporation is still lacking³⁹. It is likely that the water is released homogeneously at the nanoscale, and does not contribute to the intermittent dynamics of the speckle observed with the TRC. Nonetheless, we cannot rule out a local heterogeneous water release for plates of low mass, or close from the detachment time, while the gel is under stress. This point certainly deserves more observations with dedicated techniques in a near future.

5 Conclusion

We have described the slow aging dynamics of agar plates incubated at constant temperature. The water release leads to the delayed detachment of the gel from the sidewall of the dish. The detachment takes place sooner for plates that display a significant thickness asymmetry, while the detachment time scales quantitatively as a robust function of the gel minimal thickness, which is therefore an excellent candidate to predict the shelflife of commercial plates. To our knowledge, this study is among the first one to use speckle pattern correlation to monitor the gel contraction during syneresis and infer local information on the gel displacement dynamics. It paves the way for the use of TRC in an industrial context and more generally as a powerful tool to monitor the spontaneous or stress induced syneresis in poroelastic soft media.

Acknowledgments

The authors thank S. Manneville & M. Leocmach for fruitful discussions. This work was partially funded by the BioMérieux company.

References

- 1 R. Whistler, in *Industrial Gums: Polysaccharides and Their Derivatives*, ed. R. Whistler, Academic press INC, 1973, ch. 1, pp. 2–18.
- 2 P. Calvert, *Adv. Mater.*, 2009, **21**, 743–756.
- 3 R. Mezzenga, P. Schurtenberger, A. Burbidge and M. Michel, *Nature Materials*, 2005, **4**, 729–740.
- 4 K. Lee and D. Mooney, *Chemical Reviews*, 2001, **7**, 1869–1879.
- 5 M. Rinaudo, *Polym. Int.*, 2008, **57**, 397–430.
- 6 M. Kunitz, *J. Gen. Physiol.*, 1928, **12**, 289–312.
- 7 T. Matsushashi, in *Food gels*, ed. P. Harris, Elsevier Science Publishers LTD, 1990, ch. 1, pp. 1–51.
- 8 H. V. Dijk and P. Walstra, *Chem. Eng. J.*, 1984, **28**, 43–50.
- 9 K. Lodaite, K. Östergren, M. Paulsson and P. Dejmeck, *Int. Dairy J.*, 2001, **10**, 829–834.
- 10 M. Mellema, P. Walstra, J. van Opheusden and T. van Vliet, *Adv. Colloid Interface Sci.*, 2002, **98**, 25–50.
- 11 J. Wu, T. Yi, Y. Zhou, Q. Xia, T. Shu, F. Liu, Y. Yang, F. Li, Z. Chen, Z. Zhou and C. Huang, *J. Mater. Chem.*, 2009, **19**, 3971–3978.
- 12 T. Gan, Y. Guan and Y. Zhang, *J. Mater. Chem.*, 2010, **20**, 5937–5944.
- 13 L. Teece, M. Faers and P. Barlett, *Soft Matter*, 2010, **7**, 1341–1351.
- 14 L. Teece, J. Hart, K. N. Hsu, S. Gilligan, M. Faers and P. Bartlett, *Colloids and Surfaces A: Physicochem. Eng. Aspects*, 2014, **458**, 126–133.
- 15 K. te Nijenhuis, in *Thermoreversible networks: viscoelastic properties and structure of gels*, Springer-Verlag, Berlin, 1997, ch. 11, pp. 194–202.
- 16 M. Lahaye, *Journal of Applied Phycology*, 2001, **13**, 173–184.
- 17 N. Stanley, in *Food Polysaccharides and Their Applications*, ed. A. Stephen, G. Phillips and P. Williams, Taylor and Francis group, LLC, 2006, ch. 7, pp. 217–238.
- 18 G. Feke and W. Prins, *Macromolecules*, 1974, **7**, 527–530.
- 19 P. S. Biagio, D. Bulone, A. Emanuele, M. Palma-Vittorelli and M. Palma, *Food Hydrocolloids*, 1996, **10**, 91–97.
- 20 M. Manno, A. Emanuele, V. Martorana, D. Bulone, P. S. Biagio, M. Palma-Vittorelli and M. Palma, *Phys. Rev. E*, 1999, **59**, 2222–2230.
- 21 A. Emanuele, L. D. Stefan, D. Giacomazza, M. Trapanese, M. Palma-Vittorelli and M. Palma, *Biopolymers*, 2004, **31**, 859–868.
- 22 V. Normand, D. Lootens, E. Amici, K. Plucknett and P. Aymard, *Biomacromolecules*, 2000, **1**, 730–738.
- 23 P. Aymard, D. Martin, K. Plucknett, T. Foster, A. Clark and I. Norton, *Biopolymers*, 2001, **59**, 131–144.
- 24 D. Bulone, D. Giacomazza, V. Martorana, J. Newman and P. S. Biagio, *Phys. Rev. E*, 2004, **69**, 041401.
- 25 Z. Mohammed, M. Hember, R. Richardson and E. Morris, *Carbohydr. Polym.*, 1998, **36**, 15–26.
- 26 L. Barrangou, C. Daubert and E. Foegeding, *Food Hydrocolloids*, 2006, **20**, 184–195.
- 27 D. Bonn, H. Kelay, M. Prochnow, K. Ben-Djemia and J. Meunier, *Science*, 1998, **280**, 265–267.
- 28 S. Arnott, A. Fulmer, W. Scott, I. Dea, R. Moorhouse and D. Rees, *J. Mol. Biol.*, 1974, **90**, 269–284.
- 29 I. Dea and D. Rees, *Carbohydr. Polym.*, 1987, **7**, 183–224.
- 30 S. Boral, A. Saxena and H. Bohidar, *International Journal of Biological Macromolecules*, 2010, **46**, 232.
- 31 S. Maurer, A. Junghans and T. Vilgis, *Food Hydrocolloids*,

-
- 2012, **29**, 298–307.
- 32 D. Nordqvist and T. Vilgis, *Food Biophysics*, 2011, **6**, 45–460.
- 33 H. Deuel, G. Huber and J. Solms, *Experientia*, 1950, **6**, 138–139.
- 34 M. A. Pietranera and P. Narvaiz, *Radiat. Phys. Chem.*, 2001, **60**, 195–201.
- 35 L. Cipelletti, H. Bissig, V. trappe, P. Ballesta and S. Mazoyer, *J. Phys.: Condens. Matter*, 2003, **15**, S257–S262.
- 36 P. Snabre and J. Crassous, *Eur. Phys. J. E*, 2009, **29**, 149–155.
- 37 M. Brenner, J. Eggers, K. Joseph, S. Nagel and X. Shi, *Phys. Fluids*, 1997, **9**, 1573–1590.
- 38 E. Secchi, T. Roversi, S. Buzzaccaro, L. Piazza and R. Piazza, *Soft Matter*, 2013, **9**, 3931–3944.
- 39 G. Scherer, *Journal of Non-Crystalline Solids*, 1989, **108**, 18–27.